

**Global and regional  
aerosol optical  
thickness statistics  
and trends**

P. R. Colarco et al.

**Impact of satellite viewing swath width on  
global and regional aerosol optical  
thickness statistics and trends**

**P. R. Colarco<sup>1</sup>, R. A. Kahn<sup>2</sup>, L. A. Remer<sup>3</sup>, and R. C. Levy<sup>2</sup>**

<sup>1</sup>Atmospheric Chemistry and Dynamics Laboratory (Code 614), NASA Goddard Space Flight Center, Greenbelt, MD 20771, USA

<sup>2</sup>Climate and Radiation Laboratory (Code 613), NASA Goddard Space Flight Center, Greenbelt, MD 20771, USA

<sup>3</sup>Joint Center for Earth Systems Technology, University of Maryland-Baltimore County, 5523 Research Park Dr., Suite 320, Baltimore, MD 21250, USA

Received: 25 September 2013 – Accepted: 31 October 2013 – Published: 27 November 2013

Correspondence to: P. R. Colarco (peter.r.colarco@nasa.gov)

Published by Copernicus Publications on behalf of the European Geosciences Union.

Title Page

Abstract

Introduction

Conclusions

References

Tables

Figures



Back

Close

Full Screen / Esc

Printer-friendly Version

Interactive Discussion

## Abstract

We use the Moderate Resolution Imaging Spectroradiometer (MODIS) satellite aerosol optical thickness (AOT) product to assess the impact of reduced swath width on global and regional AOT statistics and trends. Ten different sampling strategies are employed, in which the full MODIS dataset is sub-sampled with various narrow-swath (~ 400–800 km) and curtain-like (~ 10 km) along-track configurations. Although view-angle artifacts in the MODIS AOT retrieval confound direct comparisons between averages derived from different sub-samples, careful analysis shows that with many portions of the Earth essentially unobserved, the AOT statistics of these sub-samples exhibit significant regional and seasonal biases. These AOT spatial sampling artifacts comprise up to 60% of the full-swath AOT value under moderate aerosol loading, and can be as large as 0.1 in some regions under high aerosol loading. Compared to full-swath observations, narrower swaths exhibit a reduced ability to detect AOT trends with statistical significance, and for curtain-like sampling we do not find any statistically significant decadal-scale trends at all. An across-track sampling strategy obviates the MODIS view angle artifact, and its mean AOT converges to the full-swath mean values for sufficiently coarse spatial and temporal aggregation. Nevertheless, across-track sampling has significant seasonal-regional sampling artifacts, leading to biases comparable to the curtain-like along-track sampling, lacks sufficient coverage to assign statistical significance to aerosol trends, and is not achievable with an actual narrow-swath or curtain-like instrument. These results suggest that future aerosol satellite missions having significantly less than full-swath viewing are unlikely to sample the true AOT distribution well enough to determine decadal-scale trends or to obtain the statistics needed to reduce uncertainty in aerosol direct forcing of climate.

## Global and regional aerosol optical thickness statistics and trends

P. R. Colarco et al.

Title Page

Abstract

Introduction

Conclusions

References

Tables

Figures



Back

Close

Full Screen / Esc

Printer-friendly Version

Interactive Discussion









## Global and regional aerosol optical thickness statistics and trends

P. R. Colarco et al.

Title Page

Abstract

Introduction

Conclusions

References

Tables

Figures

◀

▶

◀

▶

Back

Close

Full Screen / Esc

Printer-friendly Version

Interactive Discussion

Aqua instrument, valid at 550 nm, from the Collection 5 MODIS algorithm products (Remer et al., 2005, 2008; Levy et al., 2010). The retrievals are made at a nominal 10 km × 10 km spatial resolution at nadir. A quality assurance (QA) flag is reported for each retrieval, indicating its estimated level of confidence as a valid result, from tests performed during the retrieval process. QA flags range from 0 (lowest confidence) to 3 (highest confidence). In order to retain the highest quality MODIS data, in what follows we use only the highest confidence (QA = 3) retrievals over land, and require QA > 0 over ocean (Remer et al., 2008). The uncertainty in the MODIS AOT ( $\tau$ ) product is characterized such that one standard deviation (66 %) of the retrievals fall within  $\Delta\tau = \pm 0.03 \pm 0.05\tau$  over the ocean and  $\Delta\tau = \pm 0.05 \pm 0.15\tau$  over land relative to the AOT from coincident ground-based AERONET sun photometer network observations (Remer et al., 2005).

### 2.3 Sub-sampling AOT from the MODIS full swath

Our spatial sampling strategy is illustrated in Fig. 2, which shows an example over-ocean scene comprising a single MODIS Aqua swath. We consider the AOT retrieved across the MODIS full swath (FS), as well as several sub-sampled swaths in which we retain only the relevant portions of the full swath. Four narrow swaths (N1, N2, N3, and N4) are chosen to approximate the ~ 380 km wide swath of the Multi-angle Imaging Spectroradiometer (MISR, on the Terra spacecraft, Diner et al., 1998). We also consider a “mid-width” swath (MW) with coverage between the narrow and full swath composed of the union of N1 and N2. To approximate the curtain-like sampling of an instrument such as the Cloud Aerosol Lidar with Orthogonal Polarization (CALIOP, aboard the CALIPSO spacecraft, Winker et al., 2010) we consider the samplings C1, C2, C3, and C4, which are extracted at the center of the N1, N2, N3, and N4 swaths, respectively. We emphasize that in all that follows, we are using only MODIS AOT retrievals, sub-sampling the full dataset along the indicated narrow and curtain swaths. The sampling strategies are summarized in Table 1.

The individual retrievals are aggregated onto several regular latitude-longitude spatial grids typical of the grids used in global aerosol transport models. We consider the following spatial resolutions: (a)  $10^\circ \times 10^\circ$ , (b)  $2^\circ \times 2.5^\circ$ , (c)  $1^\circ \times 1.25^\circ$ , and (d)  $0.5^\circ \times 0.625^\circ$ . For each, the grid-averaged AOT is:

$$\tau_{\text{grid}} = \frac{\sum_{i=1}^n \tau_i \cdot q_i}{\sum_{i=1}^n q_i} \quad (1)$$

where  $\tau_i$  are the 1 through  $n$  individual AOT retrievals falling into the grid box and  $q_i$  is the QA value assigned to each retrieval. Our aggregation is thus QA weighted. Over land we have only retained QA = 3 retrievals, based on the MODIS Aerosol Product Data Quality Statement. The aggregation is performed daily. The temporally averaged (e.g., monthly, seasonal, annual) AOT at a grid box is:

$$\langle \tau \rangle = \frac{\sum_{j=1}^m \tau_{\text{grid},j} \cdot n_j}{\sum_{j=1}^m n_j} \quad (2)$$

where  $\tau_{\text{grid},j}$  is the grid average value at day  $j$  from Eq. (1) and  $n_j$  is the number of retrievals used to make  $\tau_{\text{grid},j}$ . This aggregation and weighting strategy is the same as in Remer et al. (2008) and Colarco et al. (2010).

## 3 Results

### 3.1 The sub-sampled AOT

The sub-sampled MODIS Aqua data are analyzed for the years 2003–2012. Figure 3 shows an example of the year 2010 annually averaged AOT from the full swath MODIS







## Global and regional aerosol optical thickness statistics and trends

P. R. Colarco et al.

Title Page

Abstract

Introduction

Conclusions

References

Tables

Figures

⏪

⏩

◀

▶

Back

Close

Full Screen / Esc

Printer-friendly Version

Interactive Discussion

visited because of coverage limitations, or else never encountered a good AOT retrieval because of algorithmic issues when it did overfly the grid box). Similar to Fig. 4, we show this for N1, N3, C1, and C3 sub-samples. This is revealing. The N1 and N3 figures show that, like the full-swath sampling, the narrow-swath sampling permits retrieval of AOT over most points on Earth at least once during the year. However, in some places where the full swath sampling would have made relatively few observations, the narrow-swath sampling provides no observations at all. (Fig. 7 shows, for example, the total number of retrievals in each grid cell that comprise the year 2010 full-swath annual mean.) These regions are generally where seasonal changes in surface brightness due to vegetation (e.g., the US southwest, the Sahel) or seasonal snow cover (the Tibetan Plateau) make retrieval difficult and thus less frequent. On the other hand, Fig. 6 illustrates something qualitatively different when only curtain-like sampling is obtained: it is clear that much of the Earth is never visited at all under this sampling.

In our analysis of observability, to reduce the issue of the view angle artifact discussed above we create what we call our “average-then-mask” strategy (Table 1). First, we construct monthly, seasonal, or annual mean maps of the AOT from the full swath data, effectively sampling the location at all viewing geometries obtained by MODIS. Second, we create masks that mark out the grid boxes observed by each sampling strategy over the relevant averaging period. Finally, we apply the masks to the aggregated maps of the full swath AOT. This “average-then-mask” strategy is in contrast to the “sample-then-average” strategy described in Sect. 2.3.

The results of this method provide a view of the features each sampling strategy can observe, and estimates of the mean AOT differences that are unbiased by scan angle artifacts. But it also represents a much richer data set than could be obtained from an instrument having similar retrieval capabilities to the full swath MODIS but having only narrow or curtain sampling. As a result, this method reduces significantly the difference in AOT variability measured by the different sampling strategies compared to the difference obtained using the “sample-then-average” method. This reduction in the variability is illustrated in Fig. 8, which shows again the time series of annual



Aerosol features over Iraq, Iran, Turkmenistan, Afghanistan, northern China, and the Sichuan Basin in central China are almost completely unobserved by the C1 sampling (Fig. 10a), and the pattern of the main Asian outflow over the northern Pacific is much less well defined.

For AOT trend and regional climate impact studies, quantitative differences matter. We assess the quantitative differences produced by different sampling strategies for several regions exhibiting major aerosol features as highlighted with white boxes in Figs. 9 and 10. In Fig. 11, for each of the regions highlighted in Figs. 9 and 10 we compute the time series of the difference in the regional mean AOT due to sampling. That is, for each region and season we find the full swath regional AOT and the “average-then-mask” regional AOT for each sub-sample. The  $\Delta$ AOT shown is the difference between the maximum and minimum AOT for all ten sampling strategies, including the full-swath average. Because the glint significantly impacts the sampling in the C3 and N3 sub-samples for certain regions, we also show the  $\Delta$ AOT excluding C3 and N3 (dashed lines). This restriction is especially important for the Southern Africa, African Dust, Nile River, Southeast Asia, and Asian Outflow regions. To highlight the differences between curtain-like and narrow-swath sampling we show the  $\Delta$ AOT for the full swath, C1, C2, and C4 samplings only (blue line) and for the full swath, N1, N2, and N4 samplings only (red line). For all, we additionally show the full swath AOT value and the magnitude of  $\Delta$ AOT (in all cases, the  $\Delta$ AOT excluding the C3 and N3 samples) as a fraction of the seasonal-regional full swath AOT. Finally, the  $r^2$  correlation coefficient of the  $\Delta$ AOT (again, excluding C3 and N3) with the full swath AOT and the fraction of the full swath are also indicated.

We refer to  $\Delta$ AOT as the “sampling artifact,” as it shows the uncertainty in the seasonal-regional AOT due to spatial sampling issues. We note that for all regions the  $\Delta$ AOT sampling artifact is highest for the curtain-like sampling (blue line), and so drives the sampling artifact for all sampling strategies (black dashed line). The  $\Delta$ AOT artifact is strongly affected by the glint-impacted sub-samples (C3 and N3). This is especially evident for the African dust and Asian outflow regions, where there is essentially no

## Global and regional aerosol optical thickness statistics and trends

P. R. Colarco et al.

Title Page

Abstract

Introduction

Conclusions

References

Tables

Figures

⏪

⏩

◀

▶

Back

Close

Full Screen / Esc

Printer-friendly Version

Interactive Discussion



sampling artifact if the glint-impacted sub-samples are excluded. The glint impact is also evident in Southern Africa, the Nile River, and Southeast Asia, although in these regions there remain significant sampling artifacts.

The South America region (Fig. 11a) shows significant annual and inter-annual variability in the full swath AOT, with a peak AOT of between 0.2 and 0.4 typically occurring in JAS or OND associated with seasonal biomass burning. This peak is modestly correlated ( $r^2 = 0.25$ ) with the  $\Delta$ AOT, which can be as high as 0.06. Because this region is over land, it is not significantly affected by the C3 and N3 sunglint-related sampling biases. Interestingly,  $\Delta$ AOT is uncorrelated with its fractional comparison to the full swath AOT, although as a fraction of the full swath AOT the  $\Delta$ AOT typically peaks at 40 % and can be as high as 60 %. Thus, for South America, the uncertainty in AOT due to sampling may be as much as 0.06, comprising  $\sim 15\%$  of a base magnitude as high as about 0.4, and can also represent uncertainties as great as 60 % in the regional AOT when AOT is lower.

In Southern Africa (Fig. 11b) the glint-affected C3 and N3 samplings introduce significant bias in the  $\Delta$ AOT. This is another region affected by seasonal biomass burning, with peak AOT of about 0.4 occurring in JAS. Excluding the C3 and N3 samples, the peak  $\Delta$ AOT is at most 0.03 and is weakly correlated with the full swath AOT ( $r^2 = 0.14$ ), but much more strongly with the fractional contribution ( $r^2 = 0.72$ ).

For African Dust (Fig. 11c) the C3 and N3 samplings are determinant, and excluding these, the  $\Delta$ AOT is small (approximately 0.01) and is consistently less than about 5 % of the magnitude of the full swath seasonal-regional AOT. In other words, for the African Dust region, the average-then-mask sampling does not significantly impact these AOT statistics. For the Nile River (Fig. 11d) the C3 and N3 are similarly important drivers. Excluding these, the  $\Delta$ AOT is at most about 0.05 and is modestly correlated ( $r^2 = 0.37$ ) with the full swath seasonal-regional mean AOT signal. The full swath mean AOT has a seasonal signal, varying between about 0.2 and 0.4 in magnitude, and the sampling artifact may be as much as about 20 % of the full swath value.

## Global and regional aerosol optical thickness statistics and trends

P. R. Colarco et al.

Title Page

Abstract

Introduction

Conclusions

References

Tables

Figures



Back

Close

Full Screen / Esc

Printer-friendly Version

Interactive Discussion



## Global and regional aerosol optical thickness statistics and trends

P. R. Colarco et al.

Title Page

Abstract

Introduction

Conclusions

References

Tables

Figures

⏪

⏩

◀

▶

Back

Close

Full Screen / Esc

Printer-friendly Version

Interactive Discussion

Turning to Asia, for the Indogangetic Plain (Fig. 11e), the  $\Delta$ AOT is mostly unaffected by the C3 and N3 samples. Peak values of  $\Delta$ AOT are as high as 0.1 but are uncorrelated with the full swath AOT, which itself peaks in magnitude at about 0.5. The sampling artifact may thus be as much as about 30 % of the full swath signal. Similarly, in China (Fig. 11f), the C3 and N3 samplings do not greatly affect the analysis. The  $\Delta$ AOT is as high as 0.09 and is sometimes as large 20 % of the full swath mean AOT, which itself varies between about 0.3 and 0.6 in magnitude. By contrast, the Southeast Asia (Fig. 11g) and Asian Outflow (Fig. 11h) regions are strongly impacted by the C3 and N3 sampling. Excluding these, the peak  $\Delta$ AOT values are 0.05 and 0.015, respectively. For Southeast Asia, this sampling artifact can be as large as 20 %, but is mostly less than 10 % of the full swath signal. The contribution to the Asian Outflow signal is negligible, with sampling introducing an uncertainty of only about 5 % at most for a full swath AOT that peaks above 0.4 in magnitude.

In summary, with the “average-then-mask” approach, differences are due solely to sampling, as we are only comparing the data set with sub-samples of itself, and cross-swath anomalies are removed by the averaging. In addition, the average-then-mask approach incorporates much greater sampling than actual reduced-swath instruments can obtain – about three-to-four times more samples for the narrow-swath, and about 16 times more samples for the curtain. However, significant qualitative and quantitative differences still appear in the seasonal, regional average AOT distributions; minima and maxima do not capture the extreme values, and some regional features are entirely missed. Due to the much greater sampling included in the “average-then-mask” data, results presented in Figs. 8–11 are significantly more favorable than would be produced for instruments having such spatial sampling characteristics, and thus the sampling artifacts presented in this section are effectively lower bounds. The overall magnitude of the sampling artifact is largest for the curtain-like sub-samples, as might be expected. The nature of this artifact is such that in some regions (South America, Indogangetic Plain, China) it can be as large as 60 % of the full swath AOT signal or as great as 0.1 in AOT magnitude.







## Global and regional aerosol optical thickness statistics and trends

P. R. Colarco et al.

Title Page

Abstract

Introduction

Conclusions

References

Tables

Figures

◀

▶

◀

▶

Back

Close

Full Screen / Esc

Printer-friendly Version

Interactive Discussion



worsens for the N1 sampling (Fig. 13c), with significance essentially gone over Sudan and Ethiopia, and as well being much reduced over Argentina. The patterns over ocean are still generally similar to the full swath, but the individual regions are less coherent. For the C1 sampling (Fig. 13d) the statistical significance at the 95 % confidence level is essentially gone, with nothing identifiable over land and only a hint of significance in the tropical Pacific and in a few other ocean regions. The patterns of significance for the other narrow and curtain-like samplings (not shown) are similar to the N1 and C1 shown in Fig. 13, respectively, though different in detail. N2 and C2 have somewhat better coverage over the oceans. N3 and C3 – again, because of the glint – show poor coverage over the oceans. C4 in particular has far worse coverage over the ocean than C1.

## 4 Discussion and conclusions

We have investigated the impact of spatial sampling on the statistics of the MODIS AOT. We showed significant differences in the global, annual mean AOT arrived at as a function of our sampling strategy (Fig. 5). The “sample-then-average” approach employed, however, could not disentangle the spatial sampling artifacts (which we are most interested in isolating) from the sensitivity of the MODIS AOT retrieval to viewing geometry. Subsequently, we considered instead the observability problem: where the sub-sample could have obtained aerosol retrievals, where it could not, and where—compared to the full-swath values—important differences in the regional and seasonal AOT are inferred. The “average-then-mask” approach (Sect. 3.2) mitigates biases associated with location in the MODIS swath, but greatly increases the sampling compared to an actual instrument having a narrower swath, because the full swath MODIS instrument obtains much more frequent observations of any given location than an actual narrow-swath instrument would. This approach yielded global, annual mean AOT values that were insignificantly different from the full-swath AOT values (Fig. 8), in contrast to what was shown in Fig. 5.

## Global and regional aerosol optical thickness statistics and trends

P. R. Colarco et al.

Title Page

Abstract

Introduction

Conclusions

References

Tables

Figures



Back

Close

Full Screen / Esc

Printer-friendly Version

Interactive Discussion

For several regions with important aerosol features, we calculated a “sampling artifact,” shown graphically in Fig. 11, illustrating deviations in the seasonal-regional mean AOT due to spatial sampling considerations. The sampling artifacts were small for our more ocean-influenced regions, but could be as large as 0.1 in the seasonal AOT for high-loading, near-source regions such as China and the Indogangetic Plain. As a percentage of the full-swath seasonal, regional mean AOT, the sampling artifact could be as large as 60 % (South America), and was in many places of order 20 % (China, Indogangetic Plain, Nile River). In almost all cases the magnitude of the sampling artifact was largest for the curtain-like sampling, with smaller artifacts inferred when the narrow-swath sampling was compared to the full swath, as might be expected. The “average-then-mask” strategy applied to the regional analysis discussed here is a lower bound on the actual sampling artifact because this approach actually draws from the full swath observations and simply excludes places *never* observed by the sub-sample.

We additionally investigated our ability to detect statistically significant trends in aerosol features as a function of spatial sampling. Although the signs of the trends were similar for the various sampling strategies employed, magnitudes were in some places quite different. This is attributable in part to the MODIS view angle bias, but also to differences in the spatial coverage. Again, most places on Earth are simply never observed with curtain-like sampling, including some major aerosol source regions. That reduced spatial coverage had a profound impact on the ability to assign statistical significance to the trends (Fig. 13). For example, even the widest of our sub-samples (MW) could not assign significance at the 95 % confidence level (generally used as the criterion for trend detection) to any decadal-scale trends over Amazonia or the central United States, and had reduced confidence in western Africa and India. The patterns of significance were even less coherent for the narrow-swath sampling, and were essentially gone for the curtain-like sampling. Without relying on direct comparison with the significance patterns in the full swath observations, it is not clear what could be said at all about aerosol trends from the curtain-like observations alone.

## Global and regional aerosol optical thickness statistics and trends

P. R. Colarco et al.

Title Page

Abstract

Introduction

Conclusions

References

Tables

Figures



Back

Close

Full Screen / Esc

Printer-friendly Version

Interactive Discussion



A recent paper by Geogdzhayev et al. (2013) is of particular relevance to this study, as they provided a similarly motivated analysis of the MODIS AOT data. Their approach was to develop sub-samples by aggregating individual scans *across* the MODIS swath. They argued that this removed the view angle artifact when compared to the full set of MODIS observations, vs. a comparison to along-track sampling (i.e., samples similar to our C1–4 sub-samples). This across-track sampling is illustrated for a portion of the MODIS Aqua orbit in Fig. 14a (compare with our along-track sampling shown in Fig. 2).

We implemented this sampling approach in the same framework as the along-track samplings discussed earlier, selecting five evenly spaced across-track sub-samples (L1, L2, L3, L4, and L5, with the “L” standing for “latitudinal”). The year 2010 annual mean AOT for the L1 sub-sample is shown in Fig. 14b. When compared with the full swath annual mean AOT (Fig. 3d) we see a lot of “noise” (small-scale variability) in the AOT field for the L1 sub-sample. Consistent with the earlier discussion of our along-track sub-samples, there are important aerosol features missed by this sampling, including the South American biomass burning plume and the Russian fires. Nevertheless, when the global, annual mean AOT is compared to the full swath AOT, there is essentially no difference between any of the latitudinal sub-samples and the full swath (Fig. 14c, shown for ocean, but the results are essentially the same over land). This result is consistent with Geogdzhayev et al. (2013).

When considering the seasonal-regional statistics, however, it is clear a significant spatial sampling artifact still remains in the across-track sampling, as might be expected from the small-scale variability in the map of global AOT (Fig. 14b). Figure 14d and e shows the across-track sampling seasonal-regional mean  $\Delta$ AOT for, respectively, South America and the Indogangetic Plain (compare with Fig. 11a and e). The sampling artifact  $\Delta$ AOT for the across-track sampling was indeed smaller than for our along-track, curtain-like sampling, but even so,  $\Delta$ AOT for the across-track sampling is substantial in places. Over South America, the peak  $\Delta$ AOT is about 0.04, smaller than the peak  $\Delta$ AOT of 0.06 in Fig. 11a, but over the Indogangetic Plain the artifact is roughly the same as shown in Fig. 11e. Note that these results were obtained similarly

## Global and regional aerosol optical thickness statistics and trends

P. R. Colarco et al.

Title Page

Abstract

Introduction

Conclusions

References

Tables

Figures

⏪

⏩

◀

▶

Back

Close

Full Screen / Esc

Printer-friendly Version

Interactive Discussion

to those shown in Fig. 11, from our optimistic “average-then-mask” approach. As the latitudinal sampling should obviate the MODIS view angle bias (Geogdzhayev et al., 2013), generating the seasonal-regional statistics using the “sample-then-average” approach would better represent the observations of an actual curtain instrument. When we tried this, we found the sampling artifact was actually worse in all regions (Fig. 15 for South America and Indogangetic Plain).

In Fig. 16 we show the AOT trend and statistical significance pattern for the L1 sub-sample. The global distribution of the sign of the trends is generally consistent with the full swath dataset (Fig. 12a), but there are considerable differences in coverage. The full swath observations have hundreds-to-thousands of observations per year informing a given grid box (Fig. 7), whereas the L1-type sampling has at most a few dozen (not shown). The relatively poor coverage for the L1 sampling at this resolution renders the trend statistically insignificant almost everywhere (Fig. 16b). This is also true for the other latitudinal sub-samples (not shown). The particular areas of coverage and trend magnitudes differ somewhat among the different latitudinal sub-samples, but in all cases there is almost no ability to assign statistical significance.

For completeness, we performed this same trend analysis at a coarser  $10^{\circ} \times 10^{\circ}$  spatial aggregation, compatible with the resolution of the analysis performed in Geogdzhayev et al. (2013). The AOT trends and the map of 95% statistical significance for the full swath, L1, N1, and C1 samplings are presented in Figs. 17 and 18, respectively. Results may be compared with Figs. 12, 13, and 16. The assignment of statistical significance to a detected trend is of course more robust at the coarser spatial resolution, since relatively more of these larger grid boxes have valid monthly means at the coarser spatial resolution. Thus, unlike what was seen at higher spatial resolution (Figs. 16b and 13d, respectively), at  $10^{\circ} \times 10^{\circ}$  spatial resolution it is possible to assign statistical significance more broadly for the L1 and C1 samples (Fig. 18).

Geogdzhayev et al. (2013) suggest that spatial coverage does not matter to the statistics of AOT. We strongly disagree. Their approach certainly reduces the across-track view angle bias in the MODIS AOT retrievals. For sufficiently coarse spatial and



**Global and regional  
aerosol optical  
thickness statistics  
and trends**

P. R. Colarco et al.

Title Page

Abstract

Introduction

Conclusions

References

Tables

Figures

⏪

⏩

◀

▶

Back

Close

Full Screen / Esc

Printer-friendly Version

Interactive Discussion

cloud exclusions, it would still be sampling only about  $\sim 10\%$  of the globe. In addition to aerosol amount and type, DARF depends strongly on the reflective properties of the surface over which the particles reside, most of which would be unobserved by the curtain instrument. What we do have, however, is MODIS, which represents the best available combination of broad swath, high quality, and long running coverage of satellite-based aerosol properties at our disposal. We find that the full-swath trends in our study actually match the “contextually less-biased” assimilation-grade trends in Zhang and Reid (2010), suggesting that although contextual bias can be an issue, it probably does not diminish the applicability of our conclusions.

An extension of our work here would be to explore the spatial sampling dependencies in the context of a data-assimilation grade instance of the MODIS dataset (e.g., Zhang and Reid, 2006) that has been processed to reduce as much as possible MODIS AOT artifacts. A further extension would be to perform similar sampling analyses in the context of a global aerosol transport model, which would obviate the context biases noted above and could help characterize these spatial and temporal sampling dependencies. A significant challenge in that approach, however, is to ascertain how well any aerosol transport model represents actual aerosol variability. Another approach would be to formally assimilate various sub-sampled MODIS data sets into a transport model and investigate the impact on predicted aerosol distributions and radiative forcing. These additional avenues of study would complement the work presented here.

*Acknowledgements.* This work was funded by the NASA Earth Science Division as part of the pre-formulation study for the Aerosol, Cloud, and ocean Ecosystem (ACE) Mission. We acknowledge Hal Maring, Paula Bontempi, Mark Schoeberl, David Starr, and Lisa Callahan for supporting this work. We thank Rich Ferrare, Alexei Lyapustin, Alexander Marshak, Jeffrey Reid, and Ellsworth Welton for comments on an early version of this manuscript. The image of the Mona Lisa shown in Fig. 1 was taken from the website: [https://en.wikipedia.org/wiki/File:Mona\\_Lisa,\\_by\\_Leonardo\\_da\\_Vinci,\\_from\\_C2RMF\\_retouched.jpg](https://en.wikipedia.org/wiki/File:Mona_Lisa,_by_Leonardo_da_Vinci,_from_C2RMF_retouched.jpg).

## References

- Anderson, T. L., Charlson, R. J., Bellouin, N., Boucherm, O., Chin, M., Christopher, S. A., Haywood, J., Kaufman, Y. J., Kinne, S., Ogren, J. A., Remer, L. A., Takemura, T., Tanré, D., Torres, O., Trepte, C. R., Wielicki, B. A., Winker, D. M., and Yu, H.: An “A-Train” strategy for quantifying direct climate forcing by anthropogenic aerosols, *B. Am. Meteorol. Soc.*, 86, 1795–1809, 2005.
- CCSP (US Climate Change Science Program) Synthesis and Assessment Product 2.3: Atmospheric Aerosol Properties and Climate Impacts, edited by: Chin, M., Kahn, R., and Schwartz, S., 116 pp., Washington, D.C., USA, 2009.
- Colarco, P., Da Silva, A., Chin, M., and Diehl, T.: Online simulations of global aerosol distributions in the NASA GEOS-4 model and comparisons to satellite and ground-based aerosol optical depth, *J. Geophys. Res.*, 115, D14207, doi:10.1029/2009JD012820, 2010.
- Colarco, P. R., Remer, L. A., Kahn, R. A., Levy, R. C., and Welton, E. J.: Implications of satellite swath width on global aerosol optical thickness statistics, *Atmos. Meas. Tech. Discuss.*, 5, 2795–2820, doi:10.5194/amtd-5-2795-2012, 2012.
- Diner, D., Beckert, J., Reilly, T., Bruegge, C., Conel, J., Kahn, R., Martonchik, J. V., Ackerman, T. P., Davies, R., Gerstl, S. A. W., Gordon, H. R., Muller, J.-P., Myneni, R. B., Sellers, P. J., Pinty, B., and Verstraete, M.: Multi-angle Imaging SpectroRadiometer (MISR) – instrument description and experiment overview, *IEEE Trans. Geosci. Remote Sens.*, 36, 1072–1087, 1998.
- Diner, D. J., Ackerman, T. P., Anderson, T. L., Bösenberg, J., Braverman, A. J., Charlson, R. J., Collins, W. D., Davies, R., Holben, B. N., Hostetler, C. A., Kahn, R. A., Martonchik, J. V., Menzies, R. T., Miller, M. A., Ogren, J. A., Penner, J. E., Rasch, P. J., Schwartz, S. E., Seinfeld, J. H., Stephens, G. L., Torres, O., Travis, L. D., Wielicki, B. A., and Yu, B.: PARAGON: an integrated approach for characterizing aerosol climate impacts and environmental interactions, *Bull. Am. Meteorol. Soc.*, 85, 1491–1501, doi:10.1175/BAMS-85-10-1491, 2004.
- Geogdzhayev, I., Cairns, B., Alexandrov, M., and Mishchenko, M. I.: Statistical analysis of single-track instrument sampling in spaceborne aerosol remote sensing for climate research, *J. Quant. Spectrosc. Ra.*, 121, 69–77, doi:10.1016/j.jqsrt.2013.02.003, 2013.
- Hansen, J., Rossow, W., Carlson, B., Laci, A., Travis, L., DelGenio, A., Fung, I., Cairns, B., Mishchenko, M., and Sato, M.: Low-cost long-term monitoring of global climate forgings and feedbacks, *Clim. Change*, 31, 247–271, 1995.

### Global and regional aerosol optical thickness statistics and trends

P. R. Colarco et al.

Title Page

Abstract

Introduction

Conclusions

References

Tables

Figures



Back

Close

Full Screen / Esc

Printer-friendly Version

Interactive Discussion



## Global and regional aerosol optical thickness statistics and trends

P. R. Colarco et al.

Title Page

Abstract

Introduction

Conclusions

References

Tables

Figures

⏪

⏩

◀

▶

Back

Close

Full Screen / Esc

Printer-friendly Version

Interactive Discussion

- Kahn, R. A.: Reducing the uncertainties in direct aerosol radiative forcing, *Surv. Geophys.*, **33**, 701–721, doi:10.1007/s10712-011-9153-z, 2012.
- Kiehl, J. T.: Twentieth century climate model response and climate sensitivity, *Geophys. Res. Lett.*, **34**, L22710, doi:10.1029/2007GL031383, 2007.
- 5 Levy, R. C., Remer, L. A., and Dubovik, O.: Global aerosol optical properties and application to moderate resolution imaging spectroradiometer aerosol retrieval over land, *J. Geophys. Res.*, **112**, D13210, doi:10.1029/2006JD007815, 2007a.
- Levy, R. C., Remer, L. A., Mattoo, S., Vermote, E. F., and Kaufman, Y. J.: Second-generation operational algorithm: retrieval of aerosol properties over land from inversion of moderate resolution imaging spectroradiometer spectral reflectance, *J. Geophys. Res.*, **112**, D13211, doi:10.1029/2006JD007811, 2007b.
- 10 Levy, R. C., Leptoukh, G. G., Kahn, R., Zubko, V., Gopalan, A., and Rember, L. A.: A critical look at deriving monthly aerosol optical depth from satellite data. *IEEE Trans. Geosci. Remote Sens.*, **47**, 2942–2956, doi:10.1109/TGRS.2009.2013842, 2009.
- 15 Levy, R. C., Remer, L. A., Kleidman, R. G., Mattoo, S., Ichoku, C., Kahn, R., and Eck, T. F.: Global evaluation of the Collection 5 MODIS dark-target aerosol products over land, *Atmos. Chem. Phys.*, **10**, 10399–10420, doi:10.5194/acp-10-10399-2010, 2010.
- Loeb, N. G. and Su, W.: Direct aerosol radiative forcing uncertainty based on a radiative perturbation analysis, *J. Climate*, **23**, 5288–5293, doi:10.1175/2010JCLI3543.1, 2010.
- 20 McComiskey, A., Schwartz, S. E., Schmid, B., Guan, H., Lewis, E. R., Ricchiazzi, P., and Ogren, J. A.: Direct aerosol forcing: calculation from observables and sensitivities to inputs, *J. Geophys. Res.*, **113**, D09202, doi:10.1029/2007JD009170, 2008.
- Mishchenko, M., Cairns, B., Hansen, J., Travis, L., Burg, R., Kaufman, Y., Martins, J., and Shettle, E. P.: Monitoring of aerosol forcing of climate from space: analysis of measurement requirements, *J. Quant. Spect. Rad. Trans.*, **88**, 149–161, doi:10.1016/j.jqsrt.2004.03.030, 2004.
- 25 Remer, L., Kaufman, Y., Tanre, D., Mattoo, S., Chu, D., Martins, J. V., Li, R., Ichoku, C., Levy, R. C., Kleidman, R. G., Eck, T. F., Vermote, E., and Holben, B. N.: The MODIS aerosol algorithm, products, and validation, *J. Atmos. Sci.*, **62**, 947–973, 2005.
- 30 Remer, L. A., Kleidman, R. G., Levy, R. C., Kaufman, Y. J., Tanre, D., Mattoo, S., Martins, J. V., Ichoku, C., Koren, I., Yu, H., and Holben, B. N.: Global aerosol climatology from the MODIS satellite sensors, *J. Geophys. Res.*, **113**, D14S07, doi:10.1029/2007JD009661, 2008.

## Global and regional aerosol optical thickness statistics and trends

P. R. Colarco et al.

Title Page

Abstract

Introduction

Conclusions

References

Tables

Figures

⏪

⏩

◀

▶

Back

Close

Full Screen / Esc

Printer-friendly Version

Interactive Discussion

Solomon, S., Qin, D., Manning, M., Marquis, M., Averyt, K., Tignor, M. M. B., Miller Jr., H. L., and Chen, Z.: Climate Change, 2007: The Physical Sciences Basis, Cambridge University Press, Cambridge, UK, 996 pp., 2007.

Tanre, D., Herman, M., and Kaufman, Y.: Information on aerosol size distribution contained in solar reflected spectral radiances, *J. Geophys. Res.*, 101, 19043–19060, 1996.

Tanre, D., Kaufman, Y., Herman, M., and Mattoo, S.: Remote sensing of aerosol properties over oceans using the MODIS/EOS spectral radiances, *J. Geophys. Res.*, 102, 16971–16988, 1997.

Weatherhead, E. C., Reinsel, G. C., Tiao G. C., Meng, X. L., X. L., Choi, D., Cheang, W. K., Keller, T., DeLuisi, J., Wuebbles, D. J., and Kerr, J. B.: Factors affecting the detection of trends: statistical considerations and applications to environmental data, *J. Geophys. Res.-Atmos.*, 103, 17149–17161, 1998.

Winker, D. M., Pelon, J., Coakley, J. A. J., Ackerman, S. A., Charlson, R. J., Colarco, P. R., Flamant, P., Fu, Q., Hoff, R. M., Kittaka, C., Kubar, T. L., Le Treut, H., McCormick, M. P., Megie, G., Poole, L., Powell, K., Trepte, C., Vaughan, M. A., and Wielicki, B. A.: The CALIPSO mission: a global 3-D view of aerosols and clouds, *B. Am. Meteorol. Soc.*, 91, 1211–1229, doi:10.1175/2010BAMS3009.1, 2010.

Witte, J. C., Douglass, A. R., da Silva, A., Torres, O., Levy, R., and Duncan, B. N.: NASA A-Train and Terra observations of the 2010 Russian wildfires, *Atmos. Chem. Phys.*, 11, 9287–9301, doi:10.5194/acp-11-9287-2011, 2011.

Xiong, X., Che, N., and Barnes, W. L.: Terra MODIS on-orbit spectral characterization and performance, *IEEE Trans. Geosci. Remote Sens.*, 44, 2198–2206, 2006.

Zhang, J. and Reid, J. S.: MODIS aerosol product analysis for data assimilation: assessment of over-ocean level 2 aerosol optical thickness retrievals, *J. Geophys. Res.*, 111, D22207, doi:10.1029/2005JD006898, 2006.

Zhang, J. and Reid, J. S.: An analysis of clear sky and contextual biases using an operational over ocean MODIS aerosol product, *Geophys. Res. Lett.*, 36, L15824, doi:10.1029/2009GL038723, 2009.

Zhang, J. and Reid, J. S.: A decadal regional and global trend analysis of the aerosol optical depth using a data-assimilation grade over-water MODIS and Level 2 MISR aerosol products, *Atmos. Chem. Phys.*, 10, 10949–10963, doi:10.5194/acp-10-10949-2010, 2010.

## Global and regional aerosol optical thickness statistics and trends

P. R. Colarco et al.

Title Page

Abstract

Introduction

Conclusions

References

Tables

Figures

⏪

⏩

◀

▶

Back

Close

Full Screen / Esc

Printer-friendly Version

Interactive Discussion

**Table 1.** Summary of spatial sampling strategies illustrated in Fig. 2 and summary of temporal averaging approaches.

Sample Name	Sample Width
Full Swath (FS)	~ 2300 km
Mid-Width (MW)	~ 800 km
Narrow (4 variants: N1, N2, N3, N4)	~ 380 km
Curtain (4 variants: C1, C2, C3, C4)	~ 10 km (width of MODIS pixel)
Averaging Strategy	Procedure
Sample-then-Average	<ul style="list-style-type: none"> <li>– Per orbit, sample the MODIS full swath at the indicated sub-swath</li> <li>– Aggregate sub-sample to spatial grid</li> <li>– Average aggregates to the desired time period (e.g., monthly, seasonal, annual)</li> </ul>
Average-then-Mask	<ul style="list-style-type: none"> <li>– Per orbit, aggregate the MODIS full swath to spatial grid</li> <li>– Average to the desired time period</li> <li>– Use “sample-then-average” result for relevant sub-sample/temporal average to retain or exclude grid boxes visited in sub-sample</li> </ul>

## Global and regional aerosol optical thickness statistics and trends

P. R. Colarco et al.

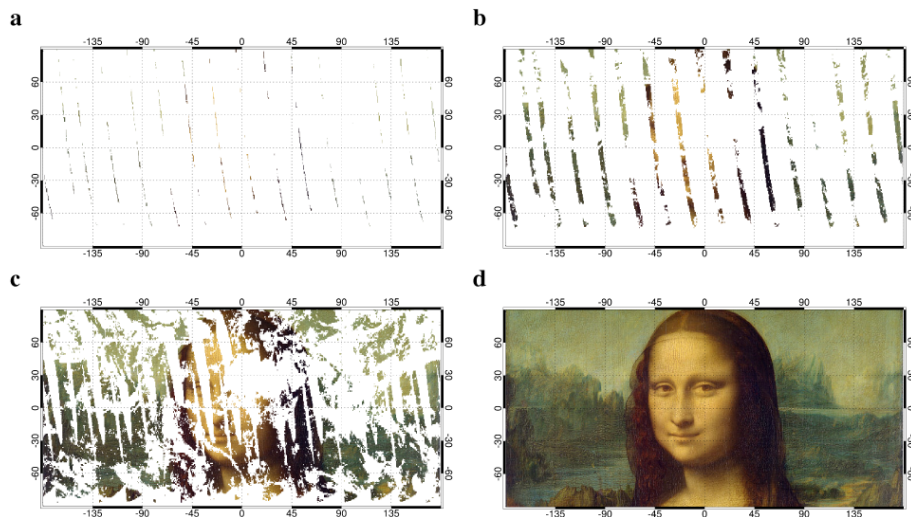


**Fig. 1.** Conceptual illustration of the spatial sampling problem. Nature presents us with a “true” scene (**d**). The truth is sampled according to a “curtain” sampling (**a**), a “narrow” sampling (**b**), and the “full swath” sampling of the MODIS instrument on the Aqua spacecraft (**c**). For purposes of this illustration we are recovering only parts of the “true” image that had valid aerosol retrievals on 5 June 2010 from the MODIS over ocean and “dark target” land retrievals.

[Title Page](#)[Abstract](#)[Introduction](#)[Conclusions](#)[References](#)[Tables](#)[Figures](#)[◀](#)[▶](#)[◀](#)[▶](#)[Back](#)[Close](#)[Full Screen / Esc](#)[Printer-friendly Version](#)[Interactive Discussion](#)



## Global and regional aerosol optical thickness statistics and trends

P. R. Colarco et al.

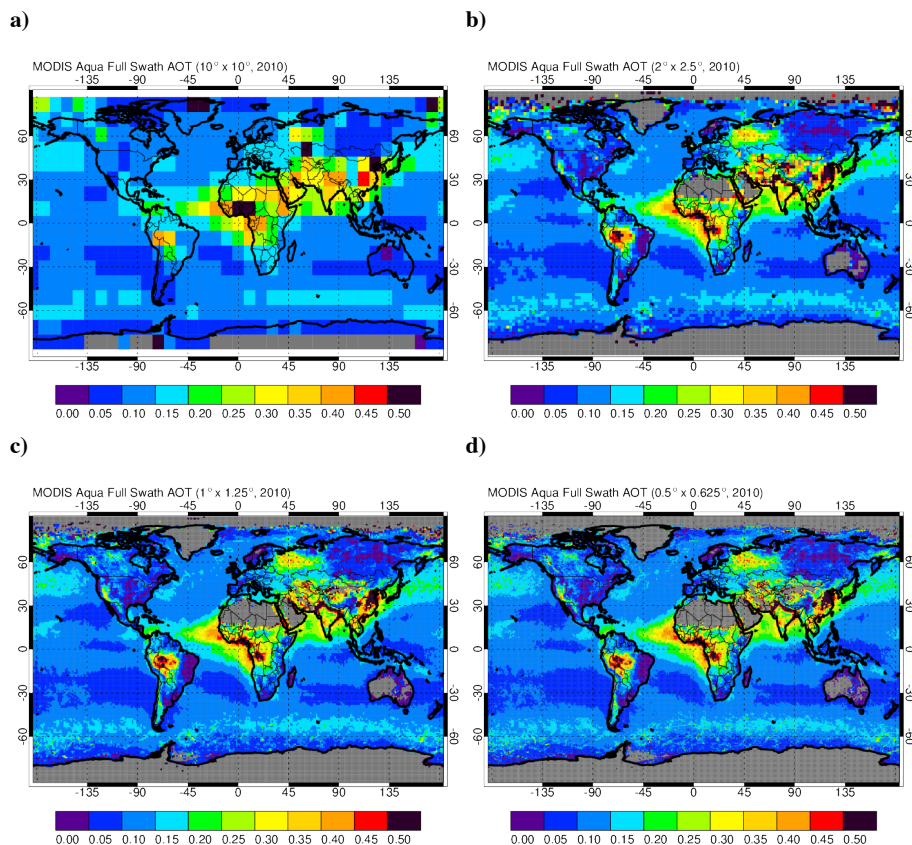


**Fig. 3.** Full swath year 2010 annual mean AOT using the sampling and aggregation strategy in Eqs. (1) and (2) for each of our four aggregation resolutions: **(a)**  $10^\circ \times 10^\circ$ , **(b)**  $2^\circ \times 2.5^\circ$ , **(c)**  $1^\circ \times 1.25^\circ$ , and **(d)**  $0.5^\circ \times 0.625^\circ$ . The grey shading indicates locations where no MODIS AOT retrievals were made during the year.

## Global and regional aerosol optical thickness statistics and trends

P. R. Colarco et al.

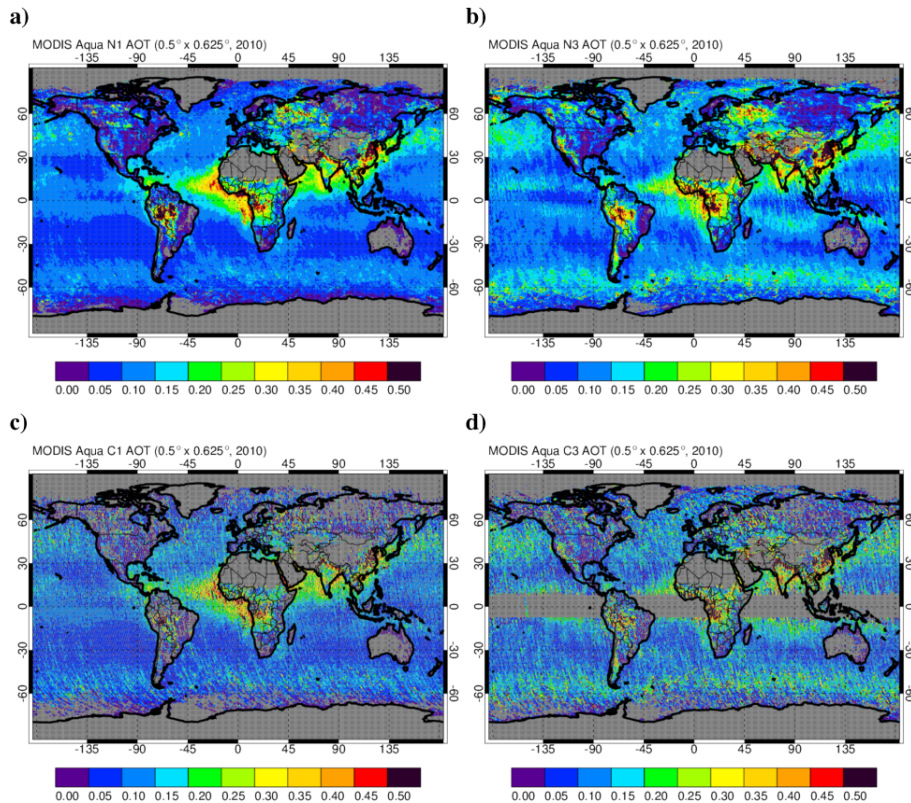


**Fig. 4.** As in Fig. 3, but at  $0.5^\circ \times 0.625^\circ$  resolution and for four of our sub-sampling strategies: (a) N1, (b) N3, (c) C1, and (d) C3.

[Title Page](#)[Abstract](#)[Introduction](#)[Conclusions](#)[References](#)[Tables](#)[Figures](#)[◀](#)[▶](#)[◀](#)[▶](#)[Back](#)[Close](#)[Full Screen / Esc](#)[Printer-friendly Version](#)[Interactive Discussion](#)

## Global and regional aerosol optical thickness statistics and trends

P. R. Colarco et al.

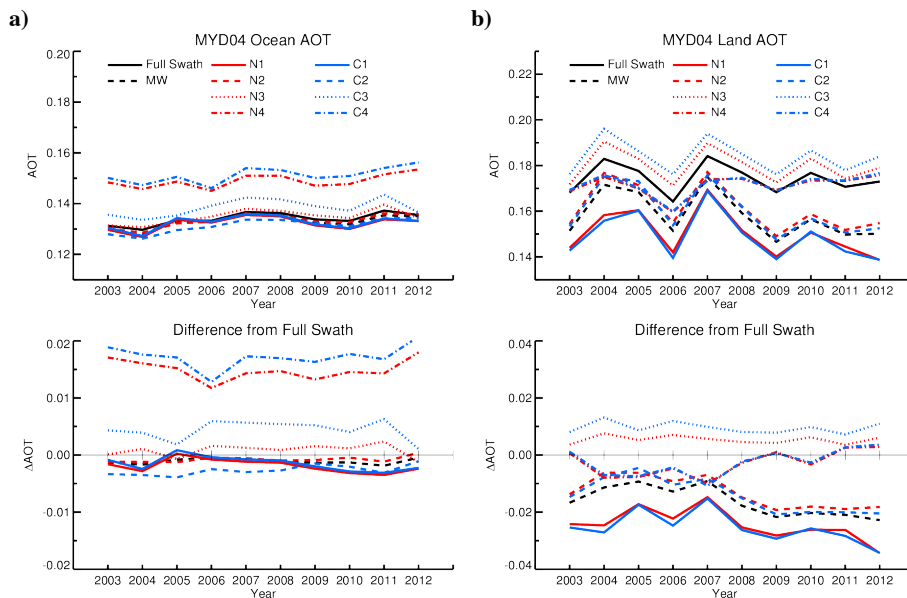


**Fig. 5.** Years 2003–2012 time series of the global, annual mean MODIS Aqua AOT over ocean **(a)** and land **(b)**. The solid black line indicates the full swath AOT, and the different colors and line styles indicate our different sampling strategies. The bottom panel in each is the difference of the sub-sampled average from the full swath average.

[Title Page](#)
[Abstract](#)
[Introduction](#)
[Conclusions](#)
[References](#)
[Tables](#)
[Figures](#)
[Back](#)
[Close](#)
[Full Screen / Esc](#)
[Printer-friendly Version](#)
[Interactive Discussion](#)

## Global and regional aerosol optical thickness statistics and trends

P. R. Colarco et al.

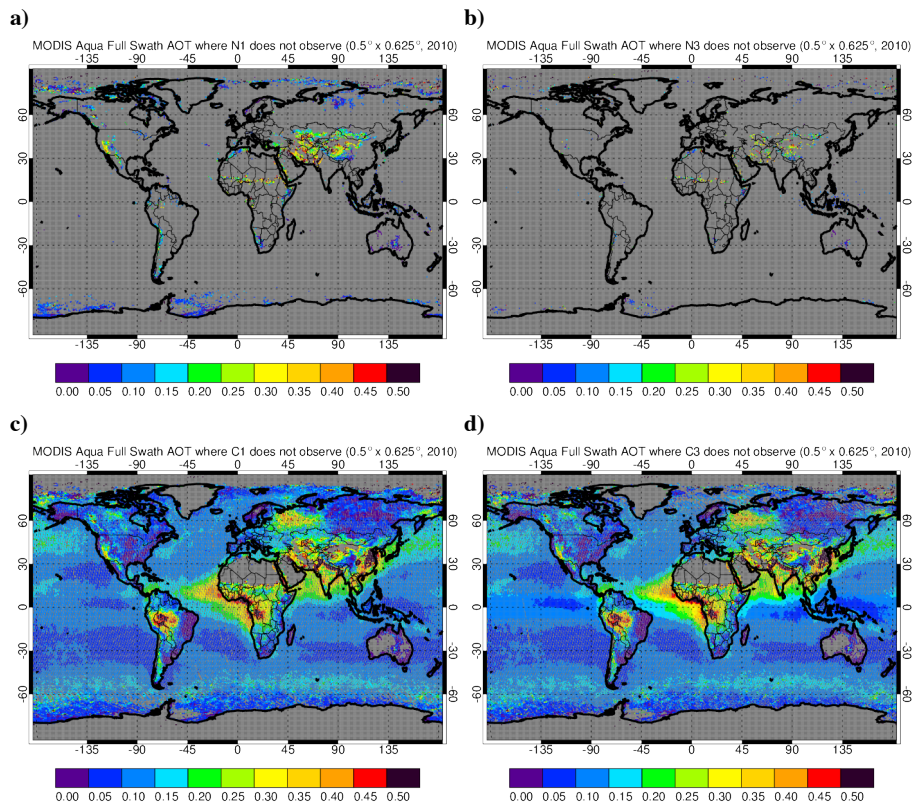


**Fig. 6.** Full swath year 2010 annual mean AOT shown only at points never sampled by the indicated sub-sample swath: **(a)** N1, **(b)** N3, **(c)** C1, and **(d)** C3.

[Title Page](#)
[Abstract](#)
[Introduction](#)
[Conclusions](#)
[References](#)
[Tables](#)
[Figures](#)
[Back](#)
[Close](#)
[Full Screen / Esc](#)
[Printer-friendly Version](#)
[Interactive Discussion](#)

## Global and regional aerosol optical thickness statistics and trends

P. R. Colarco et al.

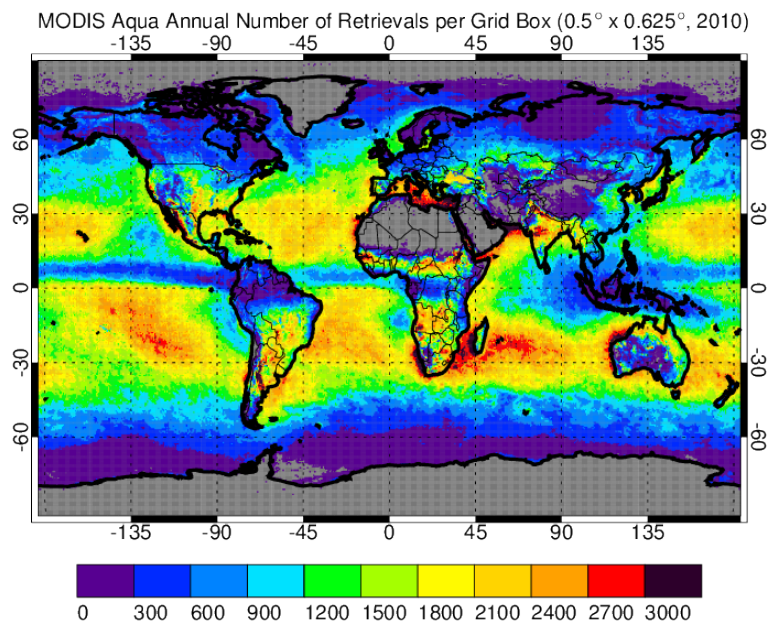


**Fig. 7.** Number of MODIS Aqua AOT retrievals made per  $0.5^\circ \times 0.625^\circ$  grid box for the entire year 2010 as used to compose the full swath annual mean shown in Fig. 3d.

[Title Page](#)[Abstract](#)[Introduction](#)[Conclusions](#)[References](#)[Tables](#)[Figures](#)[◀](#)[▶](#)[◀](#)[▶](#)[Back](#)[Close](#)[Full Screen / Esc](#)[Printer-friendly Version](#)[Interactive Discussion](#)

## Global and regional aerosol optical thickness statistics and trends

P. R. Colarco et al.

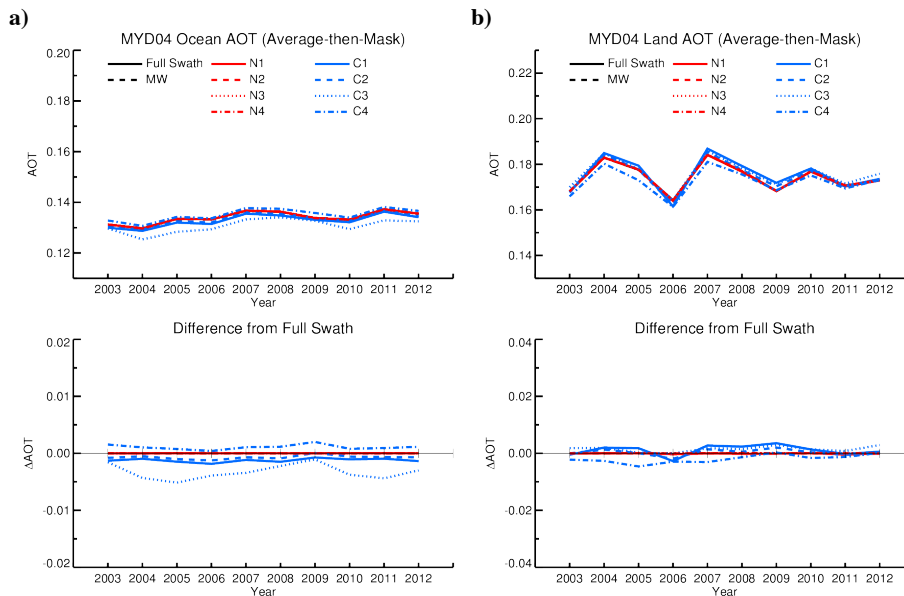


**Fig. 8.** As in Fig. 5, but now using the “average-then-mask” strategy to construct the annual means described in Sect. 3.2.

Title Page

Abstract

Introduction

Conclusions

References

Tables

Figures

⏪

⏩

◀

▶

Back

Close

Full Screen / Esc

Printer-friendly Version

Interactive Discussion



## Global and regional aerosol optical thickness statistics and trends

P. R. Colarco et al.

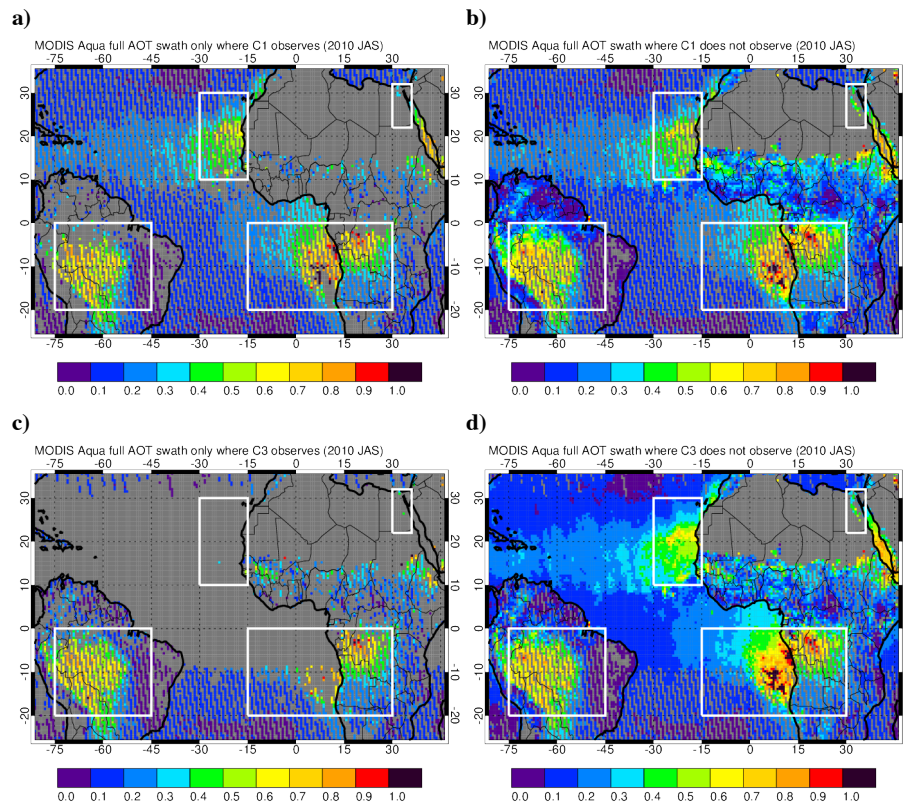


**Fig. 9.** Full swath seasonal (July-August-September 2010) MODIS Aqua AOT over the tropical Atlantic Ocean. The full swath seasonal mean is masked to show only grid cells where the C1 and C3 sub-samples do (a, c) and do not (b, d) have a seasonal mean value. Figure 9a and c illustrates the “average-then-mask” seasonal mean AOT.

## Global and regional aerosol optical thickness statistics and trends

P. R. Colarco et al.

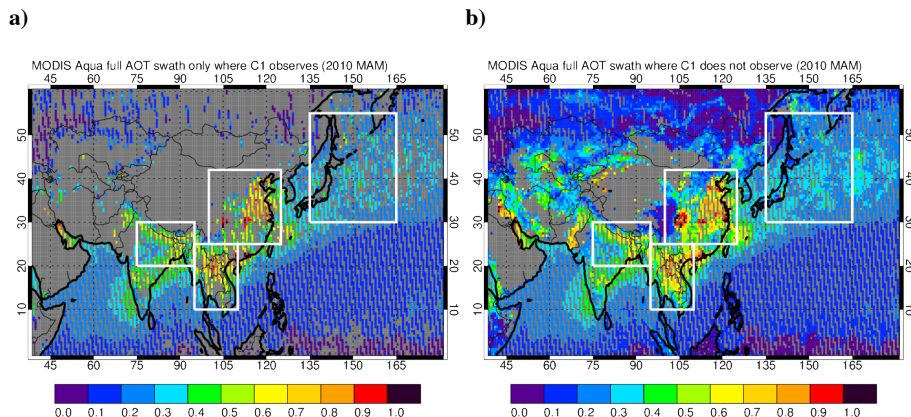
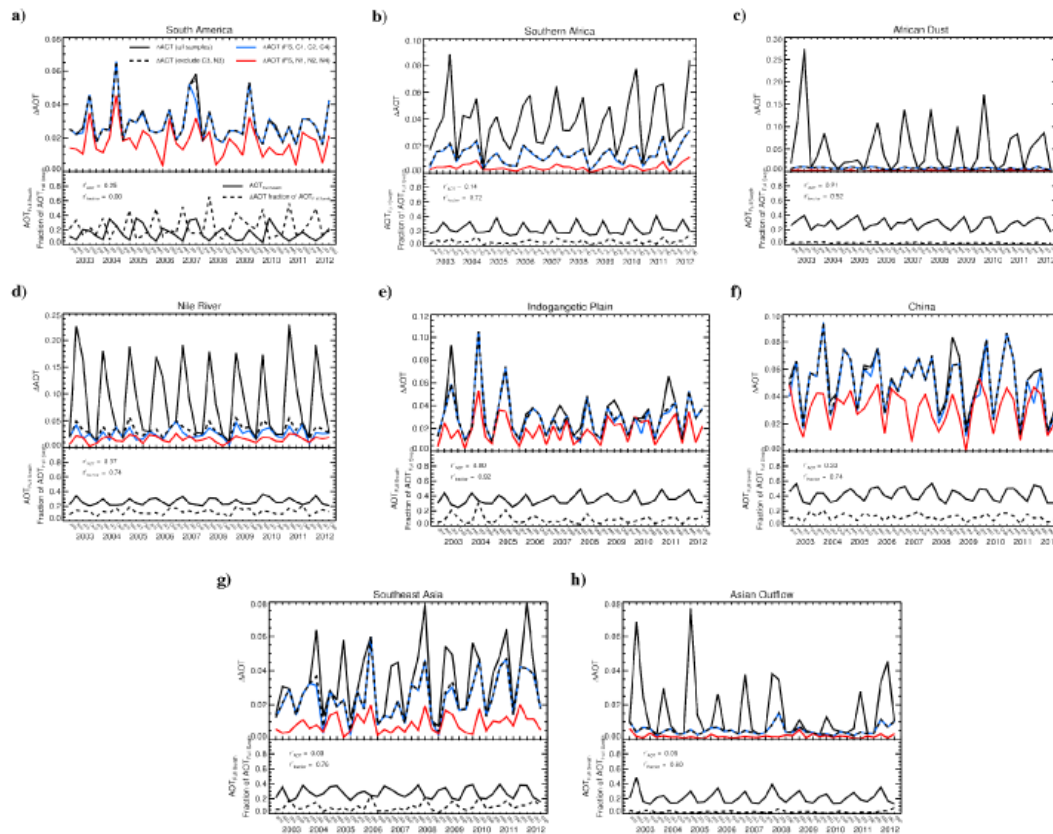


**Fig. 10.** As in Fig. 9, but for the C1 sub-sampling mask for March–April–May 2010 over Asia. The full swath seasonal mean AOT is shown both where the C1 sub-sample does (a) and does not (b) have a valid seasonal mean.

# Global and regional aerosol optical thickness statistics and trends

P. R. Colarco et al.



Title Page

Abstract

Introduction

Conclusions

References

Tables

Figures



Back

Close

Full Screen / Esc

Printer-friendly Version

Interactive Discussion

**Fig. 11.** Seasonal-regional sampling artifact as  $\Delta$ AOT between minimum and maximum AOT values for each sampling strategy (top, solid line) and for all but the C3 and N3 samples (top, dashed). For all, the “average-then-mask” sampling approach is used. The blue line is the  $\Delta$ AOT computed using only the full swath, C1, C2, and C4 samplings. The red line is the  $\Delta$ AOT using only the full swath, N1, N2, and N4 samplings. Also shown are the full swath mean AOT (bottom, solid line) and  $\Delta$ AOT as a fraction of the full swath AOT (bottom, dashed). The  $r^2$  correlation coefficient between the sampling artifact  $\Delta$ AOT (in all cases, excluding C3 and N3) the full swath seasonal-regional mean AOT and the  $\Delta$ AOT as a fraction of the full swath mean are also shown.

## Global and regional aerosol optical thickness statistics and trends

P. R. Colarco et al.

[Title Page](#)[Abstract](#)[Introduction](#)[Conclusions](#)[References](#)[Tables](#)[Figures](#)[◀](#)[▶](#)[◀](#)[▶](#)[Back](#)[Close](#)[Full Screen / Esc](#)[Printer-friendly Version](#)[Interactive Discussion](#)

## Global and regional aerosol optical thickness statistics and trends

P. R. Colarco et al.

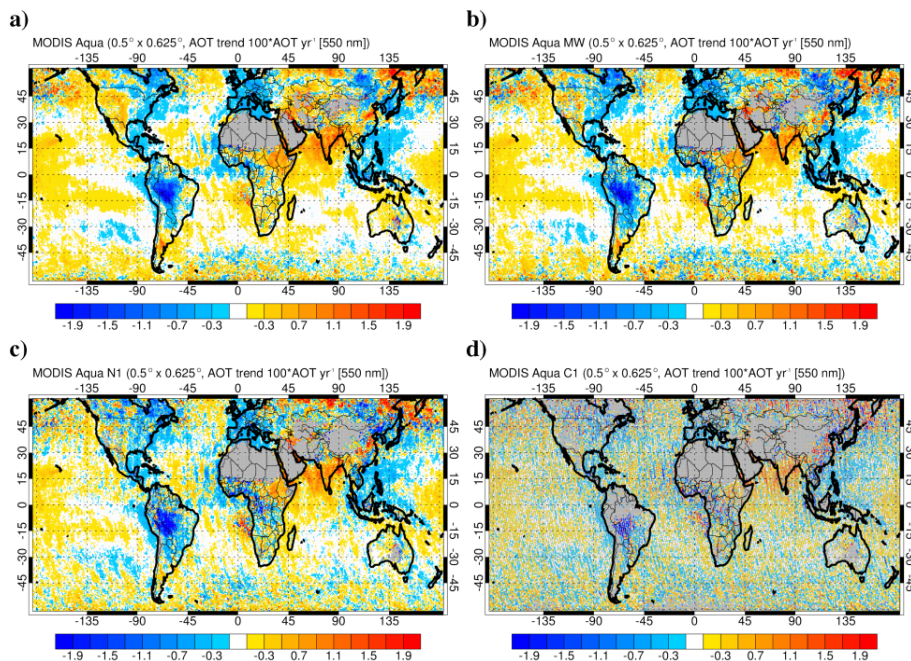


**Fig. 12.** Trend for the ten-year (2003–2012) time series of MODIS Aqua AOT. We show the trend for the full swath (a), mid-width (b), N1 (c), and C1 (d) samplings. Grey areas are locations with either no valid retrievals or where the time series has fewer than 12 month<sub>n</sub> and month<sub>n-1</sub> pairs.

Title Page

Abstract Introduction

Conclusions References

Tables Figures

◀ ▶

◀ ▶

Back Close

Full Screen / Esc

Printer-friendly Version

Interactive Discussion

## Global and regional aerosol optical thickness statistics and trends

P. R. Colarco et al.

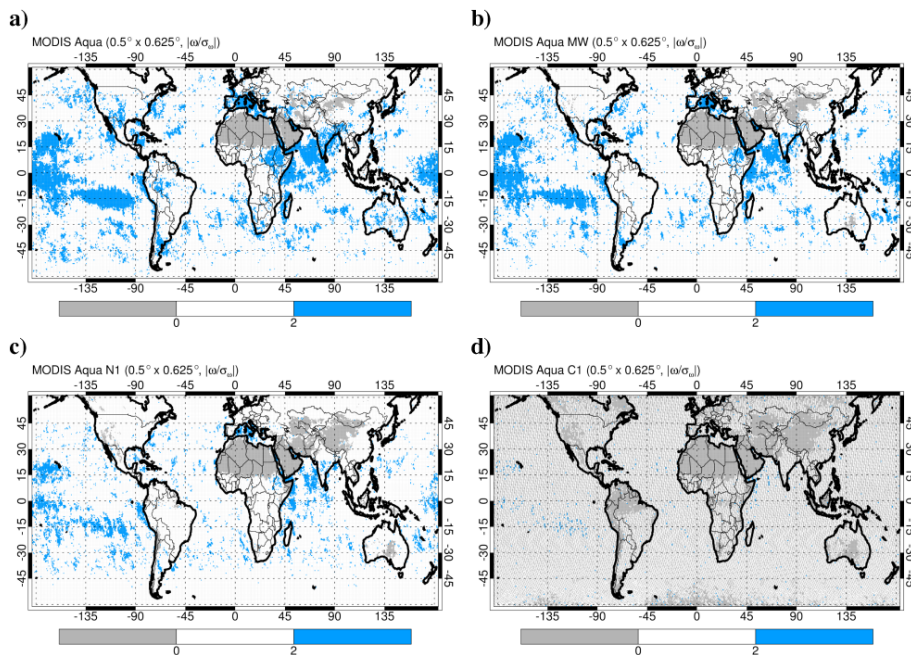


**Fig. 13.** As in Fig. 12, but showing the statistical significance for the trends shown in Fig. 12. Regions colored blue (bottom plots) are showing statistically significant trends at the 95 % confidence level.

[Title Page](#)[Abstract](#)[Introduction](#)[Conclusions](#)[References](#)[Tables](#)[Figures](#)[◀](#)[▶](#)[◀](#)[▶](#)[Back](#)[Close](#)[Full Screen / Esc](#)[Printer-friendly Version](#)[Interactive Discussion](#)

## Global and regional aerosol optical thickness statistics and trends

P. R. Colarco et al.

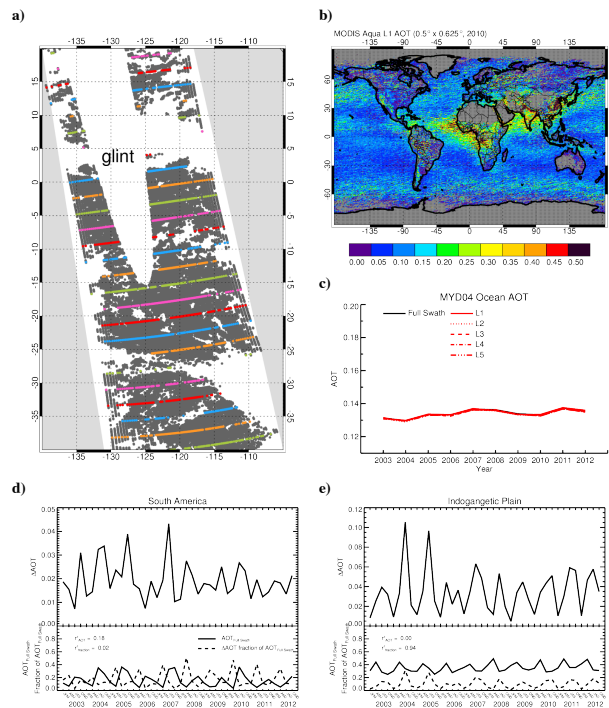


**Fig. 14.** Examples from latitudinal (across-track) sampling exercise after Geogzhayev et al. (2013). **(a)** Sampling pattern for five latitudinal sampling strategies tried: L1 (blue), L2 (orange), L3 (green), L4 (magenta), and L5 (red) (compare with Fig. 2). **(b)** Year 2010 annual mean AOT for L1 sampling (compare with Fig. 3d). **(c)** Time series of global, annual mean AOT over ocean for full swath and all latitudinal samplings (compare with Fig. 5). The full swath annual mean AOT (black line) is obscured by the latitudinal sub-samples (red lines). Also shown are the  $\Delta$ AOT sampling artifacts for two regions: South America **(d)** and the Indogangetic Plain **(e)** (compare with Fig. 11).

## Global and regional aerosol optical thickness statistics and trends

P. R. Colarco et al.

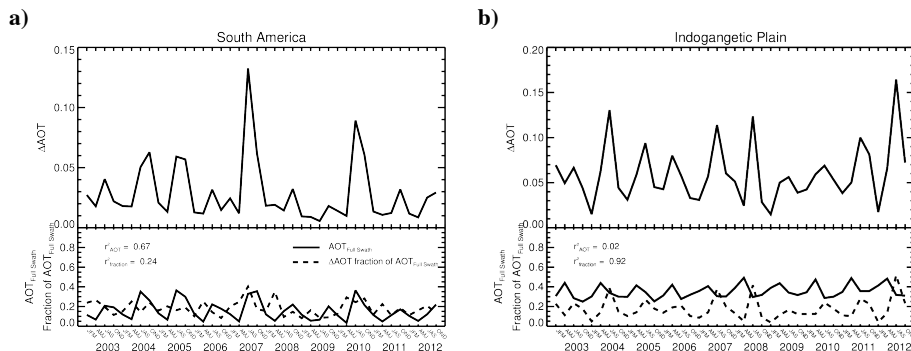


**Fig. 15.**  $\Delta AOT$  seasonal-regional sampling artifact for across-track latitudinal sampling using the “sample-then-average” approach for **(a)** South America and **(b)** Indogangetic Plain. Note the different y-axis scale from Fig. 14d and e.

## Global and regional aerosol optical thickness statistics and trends

P. R. Colarco et al.

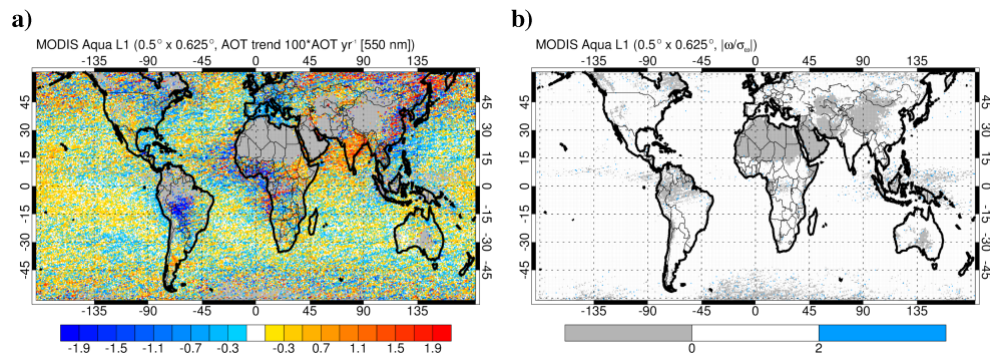


**Fig. 16.** AOT trend **(a)** and statistical significance **(b)** for the L1 across-track sub-sample.

Title Page

Abstract

Introduction

Conclusions

References

Tables

Figures

◀

▶

◀

▶

Back

Close

Full Screen / Esc

Printer-friendly Version

Interactive Discussion

## Global and regional aerosol optical thickness statistics and trends

P. R. Colarco et al.

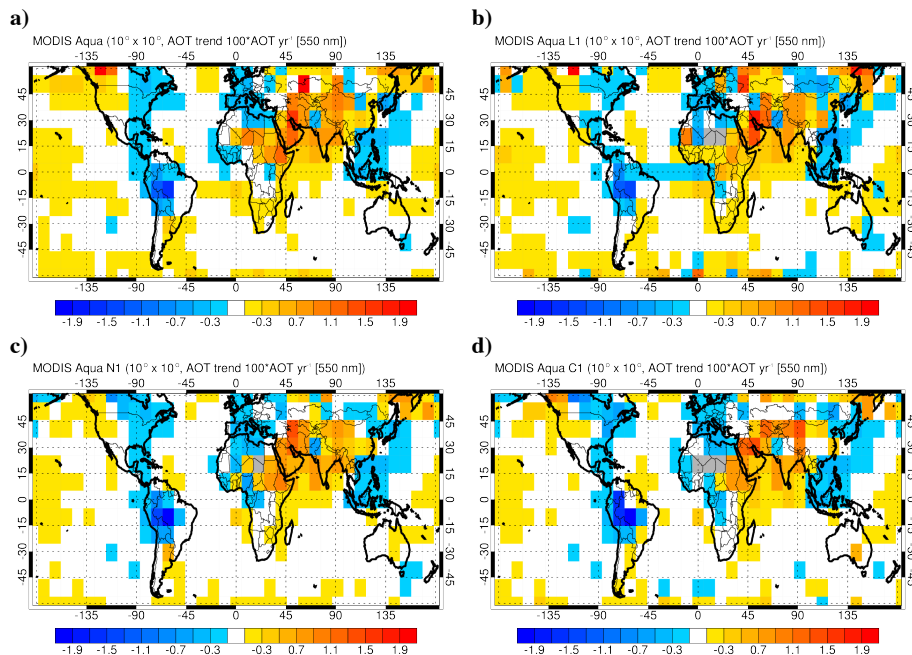


**Fig. 17.** Aerosol trends for the full swath (a), L1 (b), N1 (c), and C1 (d) samplings at  $10^\circ \times 10^\circ$  aggregation resolution.

[Title Page](#)[Abstract](#)[Introduction](#)[Conclusions](#)[References](#)[Tables](#)[Figures](#)[◀](#)[▶](#)[◀](#)[▶](#)[Back](#)[Close](#)[Full Screen / Esc](#)[Printer-friendly Version](#)[Interactive Discussion](#)

## Global and regional aerosol optical thickness statistics and trends

P. R. Colarco et al.

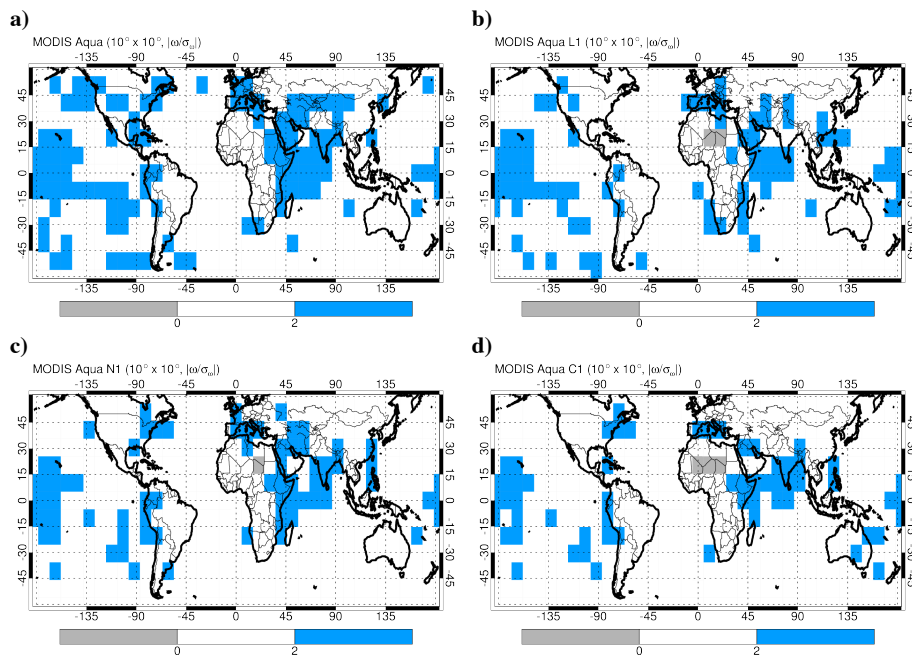


**Fig. 18.** As in Fig. 17, but for the 95 % statistical significance interval.

Title Page

Abstract

Introduction

Conclusions

References

Tables

Figures

◀

▶

◀

▶

Back

Close

Full Screen / Esc

Printer-friendly Version

Interactive Discussion